

Dynamics of Solvent Controlled ESIPT of π -Expanded Imidazole Derivatives - pH Effect

J. Jayabharathi · V. Kalaiarasi · V. Thanikachalam · K. Jayamoorthy

Received: 28 September 2013 / Accepted: 20 November 2013 / Published online: 8 January 2014
© Springer Science+Business Media New York 2014

Abstract A set of π -expanded imidazole derivatives employing excited state intramolecular proton transfer (ESIPT) was designed and synthesized. The relationship between the structure and photophysical properties were thoroughly elucidated by comparing with the analogue blocked with ESIPT functionality. The compound possessing an acidic NH function as part of an intramolecular hydrogen bond system has much higher fluorescence quantum yield and Stokes shift and the π -expansion strongly influences the optical properties. The occurrence of ESIPT for imidazole tosylamide derivatives were less affected by the hydrogen-bonding ability of the solvents compared to the unprotected amine. The low pKa values for the monocation \rightleftharpoons neutral equilibrium indicate the presence of intramolecular hydrogen bonding between the amino proton and tertiary nitrogen atom.

Keywords ESIPT · DFT · GSIPT · TICT · Monocation

Introduction

Imidazole derivatives are of continuing to attract attention due to their intriguing photophysical properties [1–14]. Photoinduced ESIPT is generally observed for organic compounds featuring both a protic acid group (e.g., OH, NH₂, NHSO₂R, etc.) and a basic site (N-, C = O, etc.) with a suitable conformation, forms an intramolecular hydrogen bond within the distance of 2.0 Å. Excited-state intramolecular proton transfer (ESIPT) phenomenon can be applied to the design of fluorescent sensors [15–20]. Typical compounds

that display ESIPT, such as benzoxazoles [21], flavones [22], 10-hydroxybenzo[h]quinoline [23] and imidazo pyridines [24], possess a large Stokes shift and hence have found applications in laser dyes [25], fluorescence recording [26], ultraviolet stabilisers [27], probes for solvation dynamics [28], biological environments [29] and recently organic light emitting devices [30]. The π -expanded multisubstituted imidazoles which exhibit ESIPT process will significantly alter their optical properties like homoaromatic systems [31–34]. Proton- and charge-transfer reactions are most fundamental processes involved in chemical reactions as well as in living systems [35, 36]. In continuation of our research [37–44] herein we present the synthesis and optical properties of π -expanded imidazole derivatives containing amino functionality combining for the first time a study of ESIPT. Also the aim of our present study are (i) to observe whether monoprotic phototautomer is formed or not, (ii) to find the site of protonation (for the formation of monocations and dications) of the molecules under study, (iii) to determine the pKa for various prototropic reactions in S₀ and S₁ states and (iv) to perform a quantum chemical calculation to explain the electronic absorption spectra of the molecules and to calculate the charge densities at the basic centres.

Experimental

Spectral Measurements

The infrared spectra were recorded with an Avatar 330-Thermo Nicolet FT-IR spectrometer. The proton spectra at 400 MHz were obtained at room temperature using a Bruker 400 MHz NMR spectrometer. Proton decoupled ¹³C NMR spectra were also recorded at room temperature employing a Bruker 400 MHz NMR spectrometer operating at 100 MHz. The mass spectra of the samples were obtained using a

J. Jayabharathi (✉) · V. Kalaiarasi · V. Thanikachalam · K. Jayamoorthy
Department of Chemistry, Annamalai University,
Annamalainagar 608002, Tamilnadu, India
e-mail: jtchalam2005@yahoo.co.in

Thermo Fischer LC-Mass spectrometer in FAB mode. The cyclic voltammetry analyses were performed with CHI 630A potentiostat-electrochemical analyzer at scan rate of 100 mV s^{-1} using 0.1 M tetra-*n*-butyl-ammonium hexafluorophosphate as supporting electrolyte with Ag/Ag^+ (0.01 M AgNO_3) as the reference electrode and Pt electrode as the working electrode under nitrogen atmosphere at room temperature. The UV-vis absorption and fluorescence spectra were recorded with PerkinElmer Lambda 35 spectrophotometer and PerkinElmer LS55 spectrofluorimeter, respectively.

Computational Details

The quantum chemical calculations were performed using the Gaussian 03 [45] package. Computations of the vertical excitations, difference density plots and optimization of the ground and excited states were performed using density functional theory (DFT) and time-dependent DFT (TD-DFT) using B3LYP/6-31G (d,p) basis set, respectively. The ground and excited states HOMO and LUMO frontier orbital's of imidazole derivatives were calculated by both DFT and TD-DFT methods at the B3LYP/ 6-31(d,p) level.

General Procedure for the Facile and Rapid Synthesis of 2-Naphthyl Imidazoles by InF_3

A mixture of Benzil (10 mmol), α -Naphthylamine (10 mmol), corresponding aldehyde (10 mmol), ammonium acetate (10 mmol) and InF_3 (1 mol %) in ethanol was refluxed at 80°C . The reaction was monitored by thin layer chromatography (TLC) and the product was purified by column chromatography using benzene: ethyl acetate (9:1) as the eluent (Scheme 1)

1-(Naphthalene-1-yl)-2,4,5-Triphenyl-1H-Imidazole (1)

M.p. 251°C , Anal. calcd. for $\text{C}_{31}\text{H}_{22}\text{N}_2$: C, 88.12; H, 5.25; N, 6.63; . Found: C, 86.89; H, 4.02; N, 5.35; ^1H NMR (400 MHz, CDCl_3): δ , 7.92 (d, $J=6.8 \text{ Hz}$, 3 H), 7.56 (d, $J=6.4 \text{ Hz}$, 6 H), 7.43 (t, $J=7.6 \text{ Hz}$, 3 H), 7.26–7.37 (m, 10 H). ^{13}C NMR (100 MHz, CDCl_3 and DMSO): δ 125.68, 127.10, 128.11, 128.27, 128.33, 128.48, 130.01, 132.92, 146.13. MS: m/z . 422 $[\text{M}^+]$.

2-(1-(Naphthalene-1-yl)-4,5-Diphenyl-1H-Imidazole-2-yl)Aniline (2)

M.p. 254°C , Anal. calcd. for $\text{C}_{31}\text{H}_{23}\text{N}_3$: C, 85.10; H, 5.30; N, 9.60; . Found: C, 85.09; H, 5.25; N, 9.56; ^1H NMR (400 MHz, DMSO): δ , 7.92 (d, $J=5.2 \text{ Hz}$, 3 H), 7.56 (d, $J=3.2 \text{ Hz}$, 6 H), 7.43 (t, $J=7.2 \text{ Hz}$, 3 H), 7.26–7.37 (m, 10 H), 11.62 (s, 1 H). ^{13}C NMR (100 MHz, CDCl_3 and

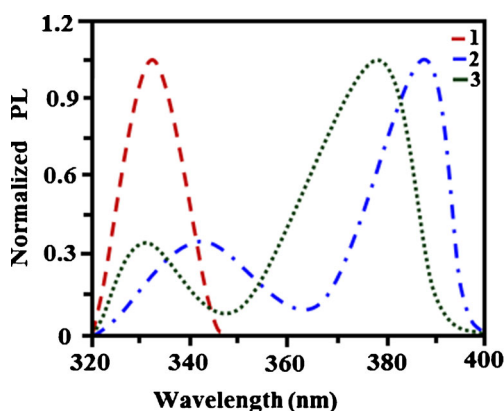
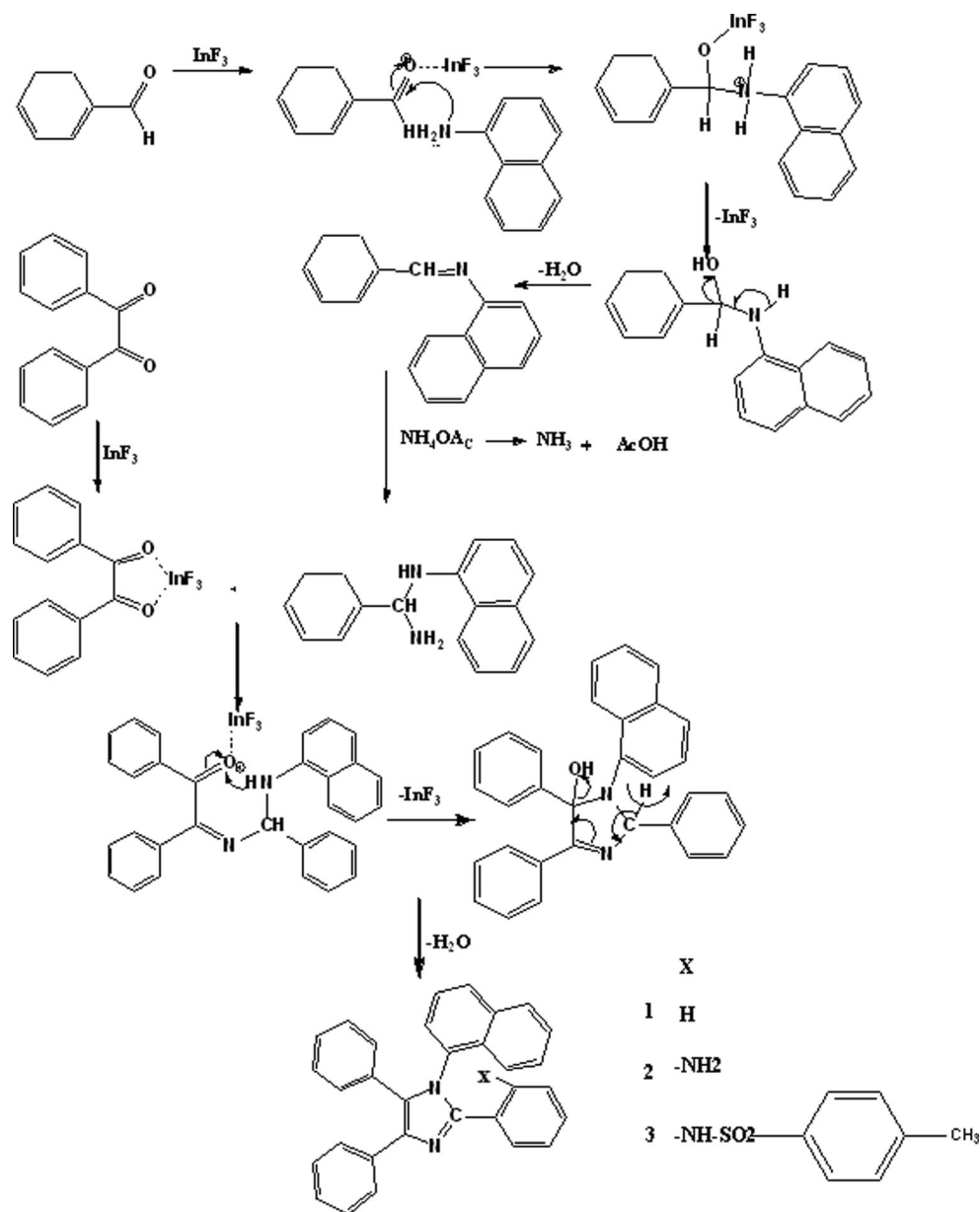
DMSO): δ 125.71, 127.28, 128.32, 128.34, 128.43, 129.51, 130.09, 132.97, 146.15. MS: m/z . 437 $[\text{M}^+]$.

4-Methyl-N-(2-(1-Naphthalen-1-yl)-4,5-Diphenyl-1H-Imidazole-2-yl)Phenyl Benzenesulfonamide(3)

M.p. 262°C , Anal. calcd. for $\text{C}_{38}\text{H}_{29}\text{N}_3\text{O}_2\text{S}$: C, 77.13; H, 4.94; N, 7.10; O, 5.41; S, 5.42; . Found: C, 77.08; H, 4.89; N, 7.03; O, 5.38; S, 5.40; ^1H NMR (400 MHz, DMSO): δ , 2.34 (s, 3 H), 6.10 (bs, 2 H), 7.93 (d, $J=3.2 \text{ Hz}$, 3 H), 7.56 (d, $J=6 \text{ Hz}$, 6 H), 7.43 (t, $J=8.8 \text{ Hz}$, 4 H), 7.27–7.37 (m, 10 H), 12.03 (s, 1 H). ^{13}C NMR (100 MHz, DMSO): δ 21.31, 125.72, 127.18, 128.31, 128.39, 128.42, 128.51, 130.09, 132.96, 136.32, 145.21, 146.23. MS: m/z . 591 $[\text{M}^+]$.

Result and Discussion

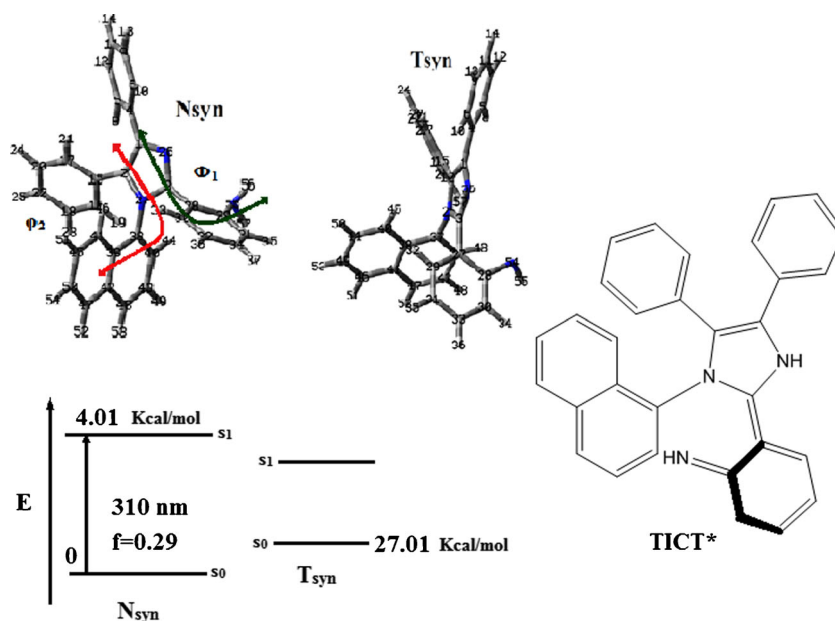
Photophysical studies of π -expanded 2-naphthylimidazoles bearing NH group as a donor in an intramolecular hydrogen bond have been carried out. The ESIPT of amino imidazoles **2** and **3** will be discussed relative to non-ESIPT compound **1**. The luminescence spectra of **1** is structured and points to a mixing with a low energy charge transfer (CT) state. The presence of such a low energy state is compatible with the presence of the electron rich amino function in **2** and **3** which might act as an electron donor toward the imidazole moiety. The observed luminescence in **2** and **3** is due to electron rich NH unit which destabilizes the CT state. However, the luminescence generated is from a state with a sizeable CT component. Accordingly, the fluorescence band shifts to a lower energy in more polar solvent which stabilizes CT. The fluorescence spectra of **2** and **3** in dioxane display a dual emission observed around 330 nm and another in bluish-green region around 370 nm (Fig. 1). This dual emission is explained as follows: the most stable form of the ESIPT molecules in the ground state is in equilibrium between different conformers (Fig. 2) arising from tautomerism and rotamerism [46]. The normal planar *syn* form (N_{syn}) features an intramolecular hydrogen bond between amino function and the basic nitrogen atom of the imidazole ring. The N_{syn} conformer can undergo proton transfer to form its tautomer (T_{syn}). Upon excitation of the normal form N_{syn} to its first excited singlet state (N_{syn}^*), undergoes an excited state intramolecular proton transfer to yield the planar tautomer (T_{syn}^*) accompanied with large Stokes' shifted fluorescence emission. The *syn*-conformers can rotamerize to form their non-planar anti forms (N_{anti} and T_{anti} , respectively). In a protic solvent, the N_{anti} conformer can form intermolecular hydrogen bonds with solvent molecules but it cannot undergo ESIPT. Therefore, dual emission is observed in non-polar solvents. In addition to the fluorescence from the T_{syn}^* and N_{anti}^* form can also exhibit normal Stokes'

Scheme 1 Synthetic route of 2-naphthyl imidazoles**Fig. 1** The fluorescence spectra of dioxane display a dual emission

shifted weak fluorescence [47, 48]. Moreover, the typical ESIPT produces the tautomeric form can be coupled with the intramolecular charge transfer (ICT) state with a rotation around interannular bond to produce a non-planar configuration (T_{ICT}^*) between the two rings. The T_{ICT}^* state can be deactivated back to its ground state via radiationless relaxation.

The existence of intramolecular hydrogen bond in **2** and **3** is confirmed by the presence of the singlets at 11.62 and 12.03 ppm respectively in the ^1H NMR spectra which is a typical signal for hydrogen bonded hydrogen atom of the ($=\text{N}\cdots\text{H}-\text{N}\equiv$). The parent compound 1-(naphthalene-1-yl)-2,4,5-triphenyl-1H-imidazole exhibits emission peak only at 332 nm. Absence of additional peak at longer wavelength

Fig. 2 Potential energy profile of N_{syn} and N_{anti} form of **2** & **3**



confirms absence of intramolecular hydrogen bond in parent compound **1**. It is further evident that intramolecular hydrogen bonding is the driving force for ESIPT and the dual fluorescence emission.

In non-polar solvents, T_{syn} form can be detected it disappears completely in alcoholic solvent, where the emission is only from the amino/CT state. Proton coupled electron transfer (PCET) reactions associated with electronically excited states is an interesting class of reactions [49] and the present case also belong to this class. Because of the introduction of the electron-withdrawing tosyl group in **3** the NH group become less electron rich due to the inductive effect of the substituent. Therefore a low energy CT excited state involving the imidazole unit is no longer possible. The difference in peak wavelength between absorption and emission is as large as 15000 cm^{-1} unambiguously supports the occurrence of ESIPT, forming a proton-transfer tautomer adiabatically in the excited state.

Quantum Chemical Calculations and Photophysical Properties

Owing to their rigid and non-coplanar structures is expected to decrease the intermolecular stacking efficiency decreases due the steric crowding. Therefore, it is expected to exhibit good solubility without loss of their excellent thermal properties. The π -expanded imidazole exhibited high melting point (T_m) around $302\text{ }^\circ\text{C}$. In addition, distinct glass transition temperature (T_g) could be observed at around $152\text{ }^\circ\text{C}$ (Fig. 3). The observed T_g and T_m values suggest that the imidazoles are amorphous nature in condensed state, which may greatly benefit the formation of homogeneous and amorphous films through thermal evaporation.

The solid state fluorescence quantum efficiency of **1–3** is around 0.48 whereas the same in solution is around 0.35.

Imidazoles **1–3** displayed a very brilliant solid film photoluminescence in the bluish-green region of the visible spectrum at room temperature. Besides electronic effect, there is probably an interesting steric effect of the multiple phenyl substituents on molecular arrangements in solid state, and is most probably interacts in an offset face-to-face fashion with another imidazolyl ring of a contiguous moiety. The relative small intermolecular π - π overlapping areas of these

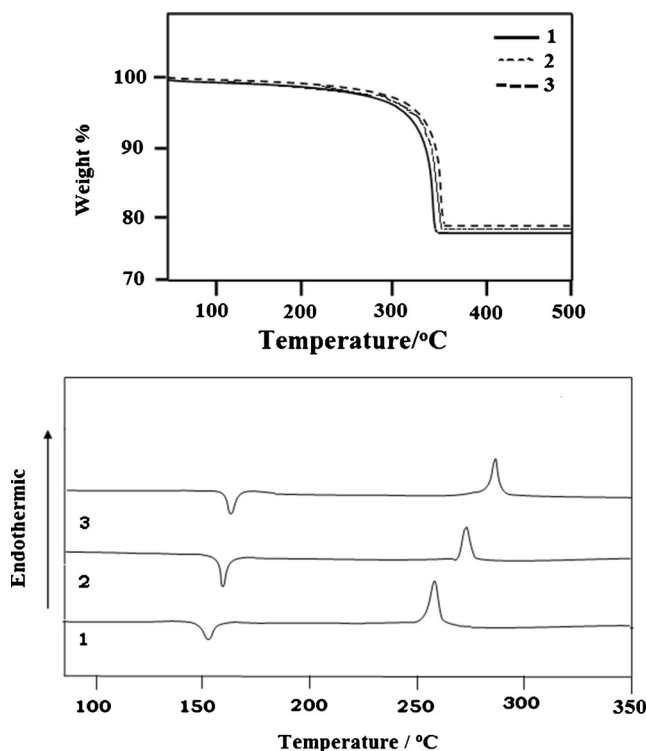


Fig. 3 TG-DTA diagram of **1–3**

imidazoles is probably a key factor that accounts for their high fluorescence quantum yield in the solid state and in the thin film. The corresponding intramolecular motions and relative free rotation of end phenyl groups in solution may be the origin of weak fluorescence. In the solid state, the free-rotation occurring in solution will be depressed due to the intermolecular interaction, which is beneficial to enhance the fluorescent efficiency.

To study further about the relationship between their molecular structures and optical properties, the geometrical parameters of $N_{\text{syn}}-T_{\text{syn}}$ tautomers and their energy-minimized, preferred conformations were calculated by DFT using B3LYP/6-31G(d,p) [46]. The geometry optimization in the S_0 and S_1 of N_{syn} , T_{syn} and their transition state (TS) of the imidazoles were performed (Table 1). The distance of $N_{26} \cdots H_{56}$ for N_{syn} form of **2** in S_0 and S_1 was about 1.78 Å. It is well known that H-bond is short distance force and hence the H-bond force between H and N should be operating in the N_{syn} form. The distance of $N_{26} \cdots H_{56}$ was too short (1.00 Å) in the

S_0 and S_1 of T_{syn} form. Generally, the $N_{\text{syn}} \rightarrow T_{\text{syn}}$ tautomerization brought a variation of the chemical bond length of amino phenyl ring. The maximum difference between the bond lengths of $N_{55}-H_{56}$ in the N_{syn} form is 0.99 Å, while in the T_{syn} form increased to 2.36 Å, implying that aromaticity of this ring in the T_{syn} form was lost because of the internal proton transfer (ESIPT) process. Again the stable ground state geometry of N_{syn} had twisted bond $\langle N_{17}-H_{52}-C_{16}-C_{36} \rangle$ by 18.1°. Dihedral angle was decreased to 2.8° during $N_{\text{syn}} \rightarrow T_{\text{syn}}$ tautomerization, reflecting that the extent of molecular distortion was reduced (Fig. 4). In a system with a great delocalization of π -electron, the torsion angle decided whether the molecule could be well-conjugated. Consequently, the small twisted configuration in the excited state allowed the extension of the conjugated π -electron in the entire molecular framework and the energy barrier in the ESIPT process caused by the ground state twisting was reduced. It was favourable to undergo ESIPT in **2** and **3**.

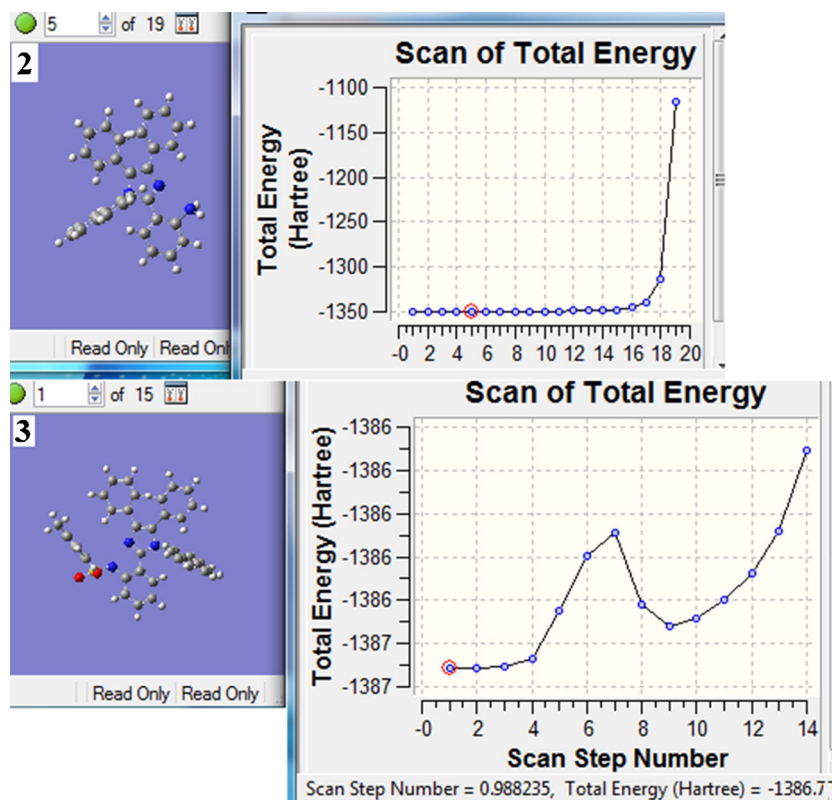
The plots of the potential curves of internal proton transfer in S_0 and S_1 states as a function of $N_{55}-H_{56}$ distance of compound **3** were performed and presented in (Fig. 5), which shows clearly that the N_{syn} form is most stable in the S_0 state whereas the T_{syn} form is most stable in the S_1 state. $\Delta E (E_{N_{\text{syn}}} - E_{T_{\text{syn}}})$ reveals that T_{syn} form has a higher energy than N_{syn} form in S_0 state as the aromatic ring is broken by proton transfer. The activation barrier for $N_{\text{syn}} \rightarrow T_{\text{syn}}$ in S_0 electronic state is 27.01 kcal mol⁻¹, large enough to make the ground state intramolecular proton transfer (GSIPT) unviable under thermal conditions, whereas upon photoexcitation, much smaller interconversion barrier ($N_{\text{syn}}^* \rightarrow T_{\text{syn}}^*$) of 4.01 kcal mol⁻¹ in S_1 state preferably allows ESIPT to give the large Stokes' shifted fluorescence emission. After decaying to the ground state, the phototautomer T_{syn}^* reverts to the original N_{syn} via reverse proton transfer barrier (ΔE_r^\ddagger) of 8.25 kcal mol⁻¹. This implied that although the occurrence of GSIPT from $N_{\text{syn}} \rightarrow T_{\text{syn}}$ should be very difficult, the reverse proton transfer process from $T_{\text{syn}} \rightarrow N_{\text{syn}}$ could take place easily, which was much favourable for ESIPT occurrence. Finally, the proton transfer from T_{syn} to N_{syn} in thermal processes in S_0 states to finish the cyclic four-level photophysical scheme ($N_{\text{syn}} \rightarrow N_{\text{syn}}^* \rightarrow T_{\text{syn}}^* \rightarrow T_{\text{syn}} \rightarrow N_{\text{syn}}$) immediately after photoexcitation of the intramolecular H-bonded molecules. Therefore, an large Stokes shift without self-absorption is detected, providing an ideal scheme for UV-photostabilizers or proton transfer lasers.

The electron distribution of the frontier orbitals reflects the electron transition characteristics (Fig. 6). The HOMO and LUMO of substituted imidazoles exhibited π -type symmetry. From HOMO to LUMO, the electron density distribution displayed the transfer from amino ring to imidazole moiety. The calculated long wavelength absorption peak around 310 nm, oscillator strength (f)=0.29 (Fig. 2) is due to a mixture of different transitions, e.g., HOMO \rightarrow LUMO,

Table 1 Selected optimized geometry parameters for the N_{syn} and T_{syn} of **2**

Geometry parameters	N_{syn}	T_{syn}
Relative energy/kcal mol ⁻¹ $S_0(S_1)$	0.00(2.02)	27.01(0.00)
Dipole moment (μ)D	3.56	8.72
Bond length (Å)		
$N_{26}-H_{56}$	1.78	1.00
$N_{55} \cdots H_{56}$	0.99	2.36
$N_{26}-C_3$	1.35	1.44
$C_{28}-C_{30}$	1.41	1.42
$C_{30}-N_{55}$	1.46	1.03
$N_{25}-C_1$	1.46	–
$N_{55}-S_{59}$	1.77	1.42
C_3-C_{28} (interannular bond length)	1.43	1.32
$S_{59}-C_{60}$	1.66	1.47
C_3-N_{27}	1.48	1.32
Bond angle (°)		
$\langle C_1-C_{26}-C_3 \rangle$	105.6	–
$\langle N_{26}-C_3-C_{28} \rangle$	123.7	125.29
$\langle N_{27}-C_3-C_{28} \rangle$	123.7	126.57
$\langle C_3-C_{28}-O_{30} \rangle$	120.2	124.43
$\langle C_{28}-C_{30}-N_{55} \rangle$	11.9	123.54
$\langle C_{30}-N_{55}-S_{59} \rangle$	112.6	118.81
Dihedral angle (°)		
$\langle N_{10}-N_{17}-C_{16}-C_{37} \rangle$	83.9	88.2
$\langle N_{17}-H_{52}-C_{16}-C_{36} \rangle$	18.1	2.8
$\langle N_{26}-C_3-C_{28}-C_{30} \rangle$	0.17	0.35
$\langle C_1-N_{26}-C_3-C_{28} \rangle$	165.7	123
$\langle C_3-C_{28}-C_{30}-N_{55} \rangle$	0.18	2.5
Excitation energy/nm	310	402
Oscillator strength (f)	0.29	0.16

Fig. 4 Molecular modeling of compound 3



HOMO \rightarrow LUMO + 1, HOMO \rightarrow LUMO + 2, etc. The LUMO electron density is delocalized through the acceptor and π -bridges. This change in the electron density acts as a driving force for the very fast intramolecular proton transfer in these compounds upon excitation to the S_1 state. Thus, the aminophenyl ring had smaller electron density in the excited state, which was the driving force for proton transfer in the excited state. Hence, the HOMO \rightarrow LUMO transition could be ascribed to π - π^* excitation with internal charge transfer character [50].

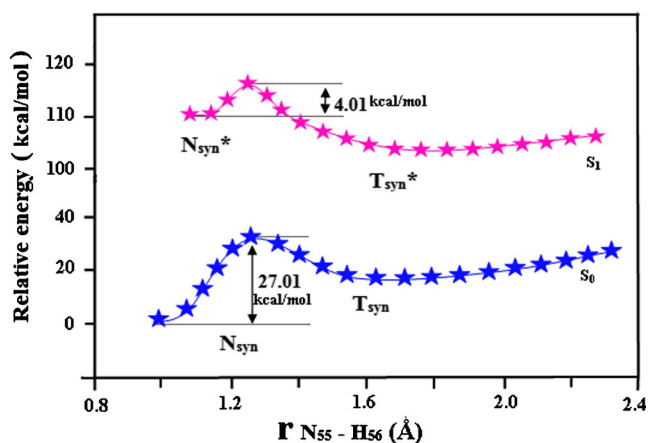


Fig. 5 Potential energy curves (PECs) of 2 & 3

The Mulliken atomic charge population of the key atoms ($N_{26}\dots H_{56}$ and $N_{55}\text{-}H_{56}$) are shown in Fig. 7. On excitation the hydrogen atom had high positive charge, which indicated that it was a real proton transfer if ESIPT took place. Interestingly, the positive charge of hydrogen experienced increasing and then decreasing during intramolecular proton transfer both in ground and excited states, reaching the maximum at transition state because of largest hydrogen-bond strength. While N_{syn} was excited to N_{syn}^* , the part of negative charge was transferred from the NH to tertiary nitrogen, which resulted in the change of the force balance of hydrogen bond. Consequently the negative charge of the proton donor decreased (more acidic) and the negative charge of the proton acceptor increased (more basic) which enhanced the change of geometry in the excited state and prompted the ESIPT occurrence for photoreactive hydrogen bonded chromophore. The ground-state dipole moment of the T_{syn} form is remarkably higher (8.72 D) than that of the N_{syn} (3.56 D). Such enlargement of dipole moment for the T_{syn} -geometry provided us the impetus to extend the calculations further so as to be able to delineate the influence of solvent reaction field on the relative stabilities of various conformers, and optimized geometry parameters. The dipole moments centralized on the Y-dimension and the electronic transition led to the changes in the charge distribution, which was accompanied by the increase of the molecular dipole moments in the excited state.

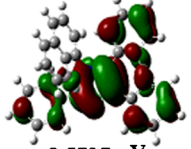
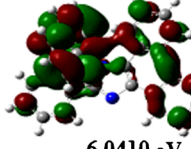
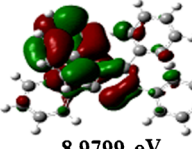
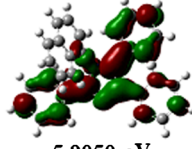
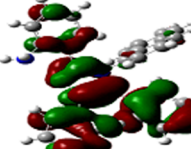
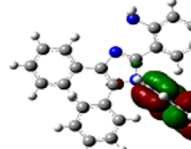
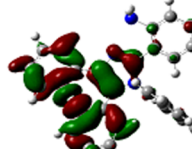
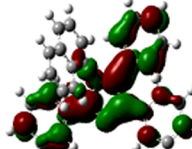
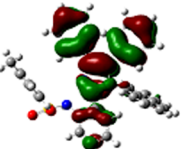
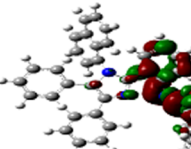
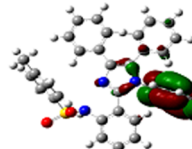
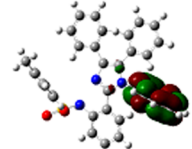
Compd.	HOMO	LUMO	HOMO-1	LUMO+1
1	 -8.5717 eV	 -6.0410 eV	 -8.9799 eV	 -5.9050 eV
2	 -8.2724 eV	 -0.7619 eV	 -8.4629 eV	 -0.5442 eV
3	 -8.4357 eV	 -0.81636 eV	 -8.5717 eV	 -0.6258 eV

Fig. 6 Frontier molecular orbitals of 1–3

MEP surface diagram is further schematic DFT evidence for the electron densities of the atoms (Fig. 8). The negative regions can be regarded as nucleophilic centres, whereas the positive regions are potential electrophilic sites. The MEP map suggests that the nitrogen atom represent the most negative potential region and the hydrogen atoms bear the maximum brunt of positive charge. The predominance of green region in the MEP surfaces corresponds to a potential halfway between the two extremes red and dark blue colour.

Restricted intramolecular/intermolecular motion [51–59] has been suggested as one of the most significant mechanisms of aggregation-induced emission enhancement phenomenon. In dilute solutions of molecular dispersed imidazole, two end-substituted units of the molecule could rotate freely around the single bonds and the radiative decay would be effectively restricted by intramolecular torsion. While in aggregate state, the intramolecular rotation and torsion were greatly impeded and therefore the non-radiative decay channel was effectively restricted and resulted in a great increase of fluorescence. Hence, it was easy to understand why the molecularly dispersed dilute solutions of imidazoles were so weakly

luminescent while their solid particles and aggregates were highly emissive. All these results in agreement with the proposed mechanism for the intramolecular H-bonded compounds 2 and 3 in dilute solution undergo an excited state charge transfer coupled proton transfer. Upon excitation of N_{syn} , an ESIPT process takes place to give T_{syn}^* fluorescent species, after which the excited tautomer undergoes a conformational change associated with a charge migration from deprotonated amino moiety to the protonated imidazole moiety, yielding the non-fluorescent charge transfer intermediate T_{ICT}^* , which probably deactivates very fast [60]. The electronic and geometric structure of T_{ICT}^* in Fig. 2 is hypothetical, not only about the nature of the conformational change experienced by T_{syn}^* but also in relation to the charge distribution. Accordingly, the fluorescence enhancement in the solid state is due to the prevented T_{ICT} by kinetic constraint which blocks the twisting motion about the interannular C-C bond along the ESIPT reaction coordinate.

The results of NBO treatment have been briefly summarized in Table 2, which reflects prominent interactions found in the N_{syn} and T_{syn} of 2 and 3 and the results for the IMHB

Fig. 7 Mulliken atomic charge population of N_{syn} , N_{syn}^* and T_{syn} forms of 3

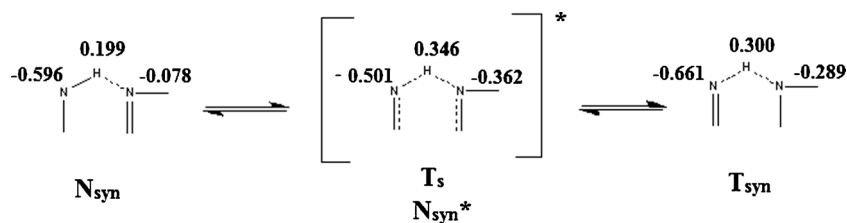
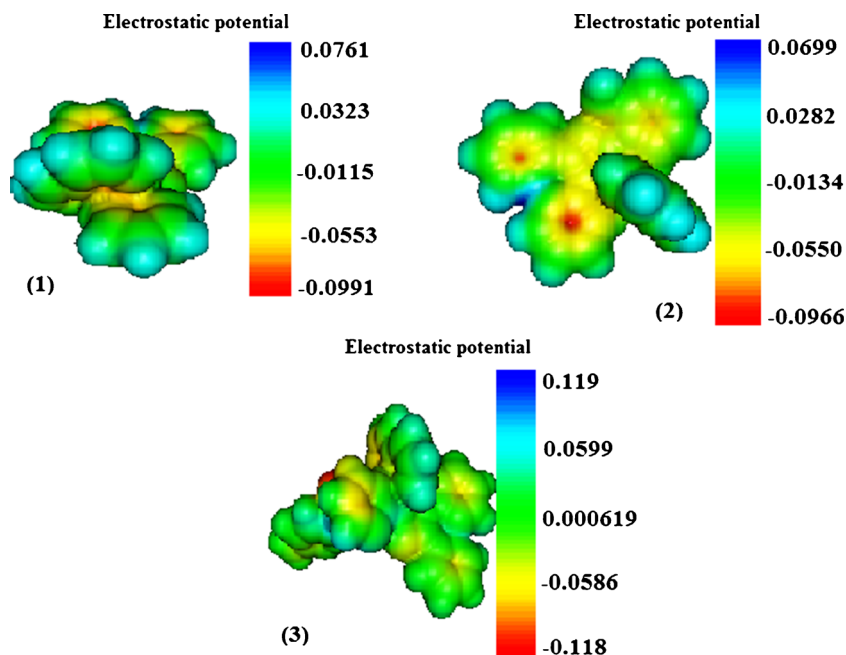


Fig. 8 MEP surface diagram of 1–3



interaction ($N_{26} - H_{56}$). The delocalization interactions are found to be especially sizeable for the π system and for the lone pairs of primary and tertiary nitrogen atoms. Table 2 dictates that in N_{syn} form the charge transfer interactions from the lone pair of electron donor (N_{26}) are directed mainly to the antibonding orbitals on the remote part of the molecule. In T_{syn} -form also, similar interactions are present to advocate for the IMHB interaction leading to the formation of six-member quasicycle [61]. Figure 9a depicts that the hyperconjugative stabilization interaction $[(\Delta E(2)_{ij})]$ between N_{26} lone pair and the $\sigma^*(N_{55}-H_{56})$ orbital is sharply diminished with elongation of the $N_{26} \dots H_{56}$ IMHB, justifying the presence of IMHB in **3**. This is a gain substantiated from the contour plot

showing the overlap between the N_{26} lone pair orbital and the $\sigma^*(N_{55}-H_{56})$ orbital (Fig. 9b). The presence of a finite, nonzero overlap between the orbitals obviously manifests

Table 2 Second order perturbation energies of some prominent interactions in the N_{syn} and T_{syn} of **2** from NBO analysis

φ_i	φ_j	N_{syn}	T_{syn}
LP N_{26}	$\sigma^*C_1-C_2$	1.88	32.43
LP N_{26}	$\sigma^*C_1-C_4$	1.57	45.95
LP N_{26}	$\sigma^*C_3-N_{27}$	5.97	21.23
LP N_{26}	$\sigma^*C_3-C_{28}$	2.32	19.56
LP N_{26}	$\sigma N_{55}-H_{56}$	29.25	–
LP N_{27}	$\sigma^*C_1-C_2$	20.67	12.23
LP N_{27}	$\sigma^*C_3-N_{26}$	23.84	18.56
LP N_{27}	$\sigma^*C_{38}-C_{39}$	3.35	8.23
LP N_{27}	$\sigma^*C_{41}-H_{46}$	1.17	9.56
LP N_{55}	$\sigma^*C_1-N_{26}$	0.61	5.23
LP N_{55}	$\sigma^*C_{28}-C_{30}$	5.35	24.56
LP N_{55}	$\sigma^*C_{30}-C_{33}$	6.27	30.85
LP N_{55}	$\sigma^*N_{26}-H_{56}$	–	24.95

(φ_i donor NBO; φ_j acceptor NBO)

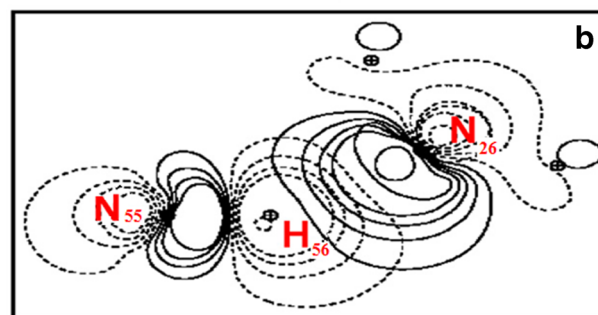
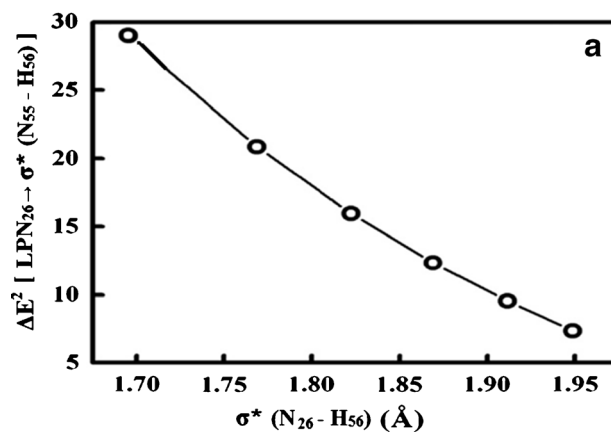


Fig. 9 a Hyperconjugative interaction energy $\Delta E^2 [LPN_{26} \rightarrow \sigma^*(N_{55}-H_{56})]$ as a function of $N_{26} \dots H_{56}$ IMHB distance for the E-form of **2** from NBO analysis. b Contour diagram of NBOs interactions between LP N_{26} and $\sigma^*(N_{55}-H_{56})$

the presence of a finite, nonzero stabilization interaction $[(\Delta E(2)_{ij})]$ due to the hyperconjugative charge transfer interaction from N_{26} lone pair to the $\sigma^*(N_{55}-H_{56})$ orbital resulting in the formation of the IMHB. Also a good extent of overlap stands in justification of a strong IMHB in **3**, in corroboration to other findings.

Effect of $[H^+]$ on Absorption and Luminescence

The absorption spectra of 1-(naphthalene-1-yl)-2,4,5-triphenyl-1H-imidazole recorded at pH 0.20 exhibits two bands, the peak at 292 nm is red shifted and the other at 251 nm is blue shifted with respect to that of the neutral molecule, 270 nm. The fluorescence spectra at different pH values are shown in Fig. 10. The fluorescence spectra obtained by exciting at the respective band maxima of the above mentioned two absorption bands are also different. Similar to the absorption spectrum, the peak at 453 nm is red shifted and the other at 403 nm is blue shifted with respect to that of the neutral molecule 420 nm. The fluorescence excitation spectrum corresponding to the blue-shifted fluorescence band matches exactly with the short wavelength absorption band while that for the red-shifted fluorescence band resembles the long wavelength absorption band. This suggests the formation of two different kinds of monocation species I and II (Scheme 2). The red-shifted absorption and emission bands correspond to the monocation I, formed by the protonation of the heterocyclic nitrogen of the imidazole ring and the blue-shifted absorption and emission bands is associated with the monocation II formed as a result of protonation at the amino nitrogen of the phenyl ring. Since the lowest energy transition of the molecule is $\pi \rightarrow \pi^*$ in nature, the protonation at the heterocyclic nitrogen atom will shift the absorption and

fluorescence bands to the red, whereas the same at the nitrogen atom of amino group will shift the band to the blue with respect to that of the neutral molecule. The large red shift for the monocation I, can be explained by the resonance interaction of the amino group with the aryl part of the molecule that leads to structure I' responsible for the stabilization of the species. The formation of both types of monocations I and II indicate the involvement of the lone pair of electrons of amino group in resonance interaction, thus reducing the charge density on the nitrogen atom and enhancing the same on the heterocyclic nitrogen atom [62].

As the pH of the medium increases pH (1.62) the intensity of the fluorescence band corresponding to species I decrease whereas that of the species II increases. Decreasing the concentration of hydrogen ions the possibility of formation of monocation I is reduced. Above pH 1.62, the intensity of the monocation II starts decreasing and at the expense of that a new band starts appearing in the wavelength 412 nm lying between the above mentioned two bands; (453 nm and 403 nm), which is almost same as λ_{max}^{fl} of TICT band in water. The appearance of TICT emission band at pH 2.18 is shown in Fig. 10, intensity of which becomes maximum at pH~3.95. All these observations supports the equilibrium [monocation II \rightleftharpoons neutral molecule III] in the pH range of 1.62–3.95. The excited state protonation constant Pk_a of this equilibrium, calculated by fluorimetric titration method [63–65] is 2.55. The monocation II shows its maximum accumulation at a pH of 1.62. With increasing pH the equilibrium concentration of the neutral species increases in the equilibrium between monocation II \rightleftharpoons neutral species III. This results an increase in fluorescence intensity of species III. When intensity of species II at pH 3.91 is very low, the intensity of species III becomes close to the intensity of species II at pH 1.62. The pK_a^* of this equilibrium is found to be 2.55, whereas the ground state protonation constant (pK_a) of the same equilibrium is 4.80. The higher value of pK_a compared to pK_a^* can be explained by the fact that basicity of N atom of amino group decreases due to a greater extent of charge transfer from the same N atom on excitation that results in the lowering of equilibrium concentration of species II in the excited state [63, 66]. The appearance of a new band at pH 2.18 suggests that this band is due to the TICT emission, which is the only predominant emission that can exist in water. This also confirms that monocation II is formed as a result of protonation of N atom of amino group, for which TICT band is not expected due to the engagement of lone pair of electrons with the H^+ ion. Therefore no TICT band appears at pH 0.20 for monocation I, although it involves greater charge transfer from N atom of amino group to the protonated imidazole ring. The protonation of N atom in this ring facilitates the conjugation of the amino group with the π -system, which in turn leads to the appearance of a double

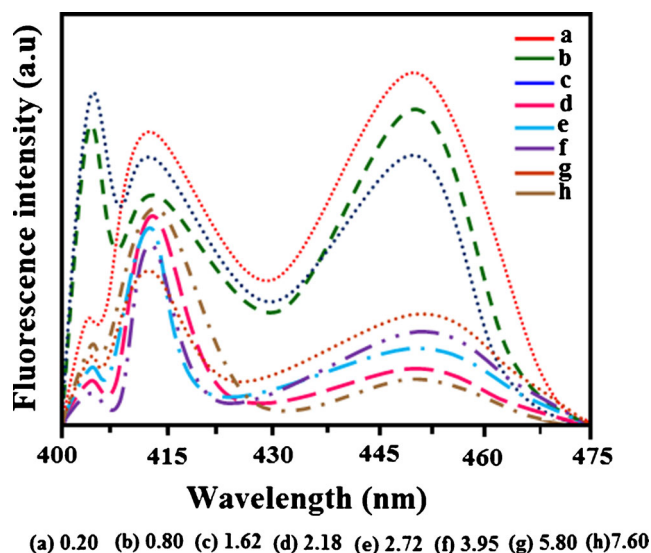
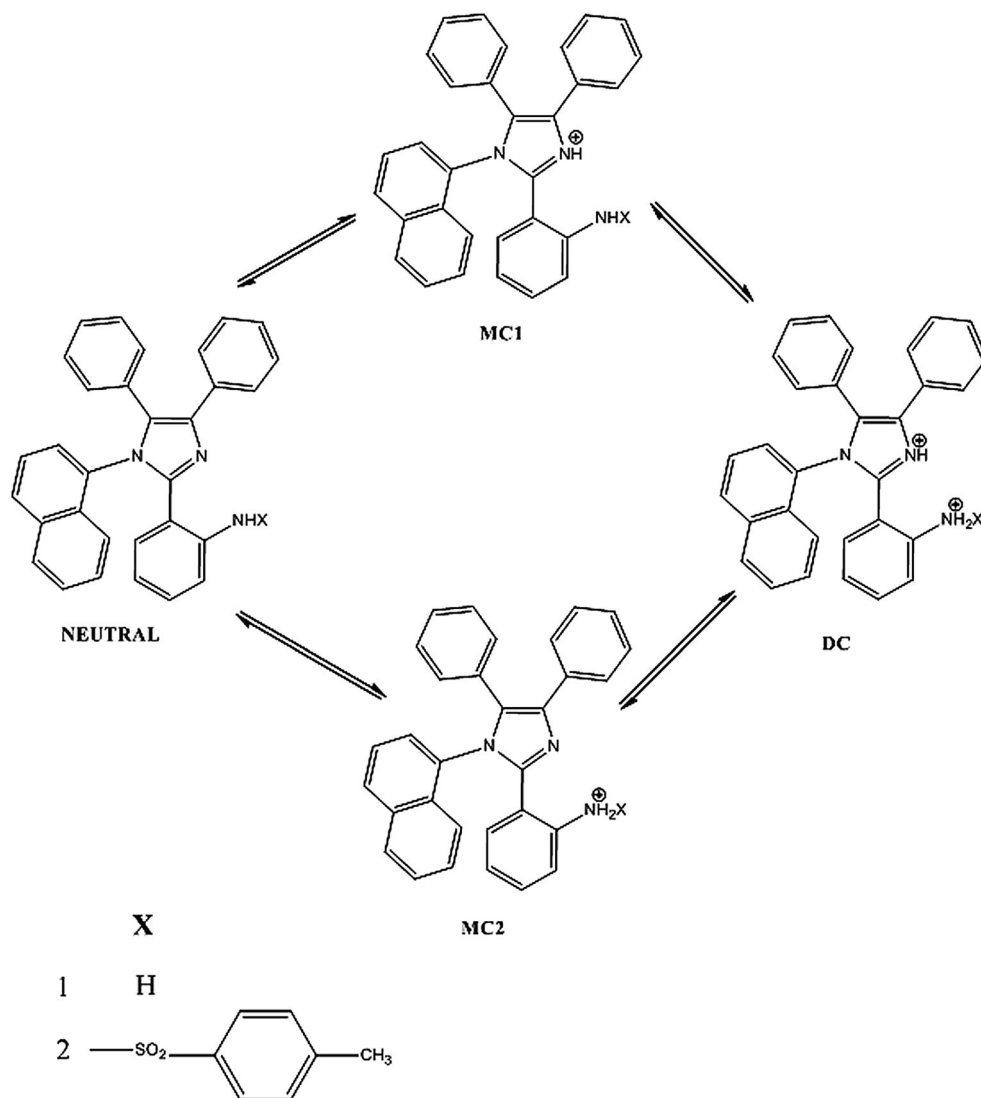


Fig. 10 Different pH values for fluorescence spectra of 1–3

Scheme 2 Formation of two different kinds of monocation species



bond character of the phenyl carbon–nitrogen bond and thus reducing the rotational relaxation of the amino group in the excited singlet state.

The TICT fluorescence intensity reaches its maximum value at pH~3.95 after which the fluorescence intensity starts decreasing and becomes constant at pH~7.0. Therefore, from this observation it can be concluded that the H-bonding effect of water becomes important only when the pH of the solution is greater than 3.95. Increasing the pH of the solution above 3.95 drives more and more H₃O⁺ ions to lose a proton to form H₂O. As a consequence the efficiency of H-bonding interactions increases, thus decreasing the TICT fluorescence intensity, which attains its minimum constant value at around pH 7.0. This observation indicates the sensing efficiency towards H-bonding interaction [67]. pK_a and pK_a^* values of monocation $\text{II} \rightleftharpoons$ neutral species equilibrium have been calculated and compared. Moreover, the fluorescence quenching of neutral molecule has been observed above pH 3.95 and the possible reason behind the same has been explained above.

Quantum Chemical Calculations Vs TICT

To rationalize the experimental findings and also to locate the TICT state, DFT calculations [67–71] have been carried out to determine the optimized geometries of the different conformations of **2** and **3** to explain their properties in the ground and excited states. When the donor-acceptor moieties orbitals are decoupled due to twisting of amino (**2**) and tosylamide (**3**) groups then full intramolecular charge transfer (ICT) takes place in the excited state. In the ground state the amino group shows a pyramidal shape because of the sp³ hybridization of the nitrogen atom and changes to trigonal planar in the excited state due to a change in hybridization of the nitrogen atom to sp² [72]. DFT calculation suggests the requirement of twisting of donor group perpendicular to the plane of the rest of the molecule for the formation of stable TICT state in polar medium. In this process the overlapping orbitals in the planar geometry get decoupled and as a result of that complete charge transfer takes place.

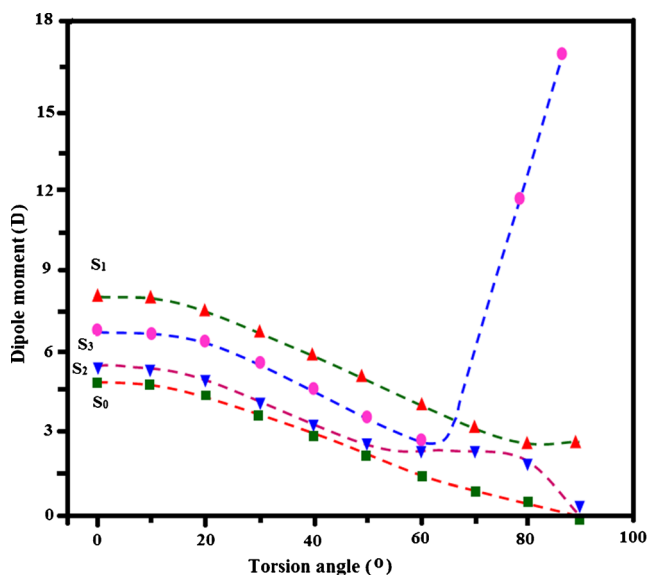


Fig. 11 Dipole moments of different singlet states with variation of the torsion angle

The formation of TICT state can be well examined through energy evolutions of several excited singlet states as a function of twist angle (φ) between the donor and acceptor parts of the molecule. Such an examination allows ascertaining the dual fluorescence and can be interpreted in terms of TICT state [71–78]. The remarkable lowering the energy of S_3 state has been observed at twist angle, $\varphi = 90^\circ$, which is consistent with increase in dipole moment (17.02 D) of the S_3 state (Fig. 11). The effect of polar solvent results in lowering the energy of S_3^{TICT} state even lower than S_1^{LE} as well as S_1^{TICT} states, which makes S_3^{TICT} state responsible for anomalous fluorescence at a critical polarity. These calculations suggest the presence of TICT state and highly Stokes shifted fluorescence in polar solvents and also support the experimental observations [79, 80].

Further formation of TICT can be confirmed by frontier molecular orbital (FMO) pictures (Fig. 6). In the planar geometry, the HOMO and LUMO have considerable delocalization over whole π -system. Both orbitals are primarily

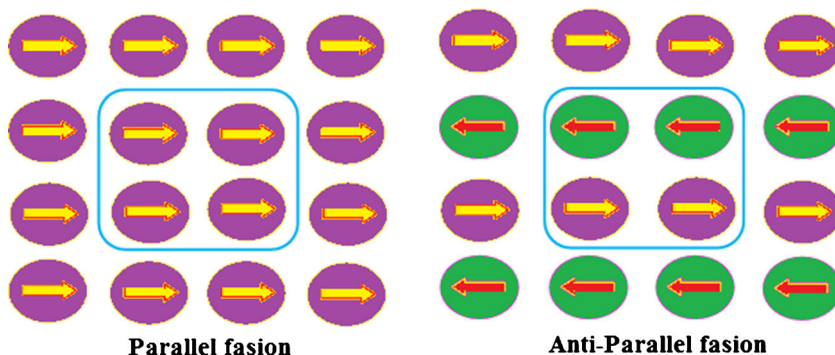
Table 3 Electric dipole moment (μ , D), polarizability (α , 10^{-30} esu) and hyperpolarizability (β_{tot} , 10^{-32} esu) of N_{syn} and T_{syn} forms of **3** from NLO analysis

S.No.	Parameters	N_{syn}	T_{syn}
1	Dipole moment	3.56	8.72
2	Polarizability	4.82	7.56
3	Hyperpolarizability	46.8	5.96
4	r	43.82	230.82
5	$\mu\beta_0$	168.93	43.68

located on the donor and acceptor parts of the molecule. The $S_0 \rightarrow S_3^{\text{LE}}$ transition occurs only with a fraction of a full electron transfer from nitrogen atom of amino function to the remainder of the molecule, which results in a calculated dipole moment at S_3^{LE} state. At the molecular twist of 90° , π orbitals of amino group are completely decoupled from the remaining π orbitals, so that the HOMO \rightarrow LUMO excitation entails a full electron transfer from the donor to the acceptor. This leads to the formation of the S_3^{TICT} state with a very high dipole moment of 17.02 D which on stabilization due to solvation with a high polar solvent and becomes responsible for the highly Stokes shifted fluorescence. In the gas phase, the energies of TICT states are greater than the respective planar S_1 and S_2 states, whereas the energy of S_3^{TICT} state is lower than the S_3 planar state. The dipole moment of only the S_3^{TICT} state among the first four singlet states is greater than the respective planar state. This dipole moment is large enough relative to the dipole moments of the remaining states to locate the TICT state by the dielectric continuum estimation in polar solvents [81].

The electrostatic first hyperpolarizability (β) and dipole moment (μ) of the imidazole chromophore have been calculated by using Gaussian 03 [45] and displayed in Table 3. The studied imidazole chromophores show larger $\mu_g\beta_0$ value, which is attributed to the positive contribution of their conjugation. The reported chromophores exhibit larger non-linearity and its λ_{abs} is shifted when compared with

Fig. 12 The parallel & anti parallel alignment of the molecular dipole moments



unsubstituted imidazole. Therefore, it is clear that the hyperpolarizability is a strong function of the absorption maximum. The observed positive small ρ^{2D} value (0.18) reveals that the β_{iii} component cannot be zero and these are dipolar component. Since most of the practical applications for second order NLO chromophores are based on their dipolar components, this strategy is more appropriate for designing highly efficient NLO chromophores. The overall polarity of the synthesized imidazole derivatives was small when their dipole moment aligned in a parallel fashion [82] (Fig. 12).

Conclusions

This article presents a facile synthesis of novel bluish-green fluorescent π -expanded imidazole derivatives and their optical, electrochemical, and thermal properties. The π -expanded branched imidazoles are more emissive, both in solution and when aggregated, presumably because of increased π -electron contributions to the electronic structure of the molecule, as well as restricted non-radiative deactivation resulting from less facile rotational deactivation via the interannular C-C bond [$<N_{17}-H_{52}-C_{16}-C_{36}$]. The quantum chemical studies reveal that the formation of non-fluorescent isomers (T_{ICT}^*) was effectively suppressed in the solid state due to the bulky substituents preventing a large-amplitude conformational change in the excited-state. The low pK_a value for the mono-cation \rightleftharpoons neutral equilibrium indicate the presence of intramolecular hydrogen bonding between the amino-proton and tertiary nitrogen atom. The ESIPT amino imidazoles containing branched groups showed excellent thermal properties with high T_g (82.3 °C) and an efficient large Stokes' shifted emission with very high fluorescence quantum yield. The molecular design concept established in this study provide guidelines for fine-tuning the emission properties of this class of ESIPT fluorophore, which is beneficial for developing a new class of advanced optoelectronic applications and biological imaging.

Acknowledgments One of the authors Prof. J. Jayabharathi is thankful to DST [No. SR/S1/IC-73/2010], DRDO (NRB-213/MAT/10-11) and CSIR (NO 3732/NS-EMRII) for providing funds to this research study.

References

- Grimmet MR, Katritzky AR, Rees CW (1984) Comprehensive heterocyclic chemistry, vol 5. Pergamon, New York, p 457
- Grimmet MR, Katritzky AR, Rees CW, Scriven EFV (1996) Comprehensive heterocyclic chemistry II, vol 3. Pergamon, New York, p 77
- Molina P, Tarraga A, Oton F (2012) *Org Biomol Chem* 10:1711
- Debus H (1858) *Liebigs Ann Chem* 107:199
- Radziszewski B (1882) *Chem Ber* 15:1493
- Hayashi T, Maeda K (1962) *Bull Chem Soc Jpn* 35:2057
- Hayashi T, Maeda K, Shida S, Nakada K (1960) *J Chem Phys* 32:1568
- Zimmerman H, Baumgartel H, Bakke F (1961) *Angew Chem* 73:808
- Blinder SM, Peller MJ, Lord NW, Aamodt KC, Ivanchukov NS (1962) *J Chem Phys* 36:540
- Igarashi H, Igarashi T, Sagawa M, Mori T, Kotani Y, Muroya Y, Katsumura Y, Yamashita T (2007) *J Photopolym Sci Technol* 20:757
- White EH, Harding MJC (1965) *Photochem Photobiol* 4:1129
- Philbrook GE, Maxwell MA, Taylor R, Totter G (1965) *Photochem Photobiol* 4:1175
- Park S, Kwon OH, Kim S, Park S, Choi MG, Cha M, Park SY, Jang DJ (2005) *J Am Chem Soc* 127:10070
- Park S, Kwon JE, Kim S-H, Seo J, Chung K, Park S-Y, Jang D-J, Medina BM, Gierschner J, Park S-Y (2009) *J Am Chem Soc* 131:14043
- Kwon JE, Park S-Y (2011) *Adv Mater* 23:3615–3642
- Fang C, Frontiera NN, Tran R, Mathies RA (2009) *Nature* 462:200–204
- Douhal A, Lahmani F, Zewail AH (1996) *Chem Phys* 207:477
- Kim JS, Quang DT (2007) *Chem Rev* 107:3780
- Wang B, Eric V, and Anslyn EV (2011) *Chemosensors: Principles, strategies, and applications*. Wiley pp. 253–273
- Roshal AD, Grigorovich AV, Doroshenko AO, Pivovarenko VG (1998) *J Phys Chem A* 102:5907
- Mordzinski A, Grabowska A, Kuhnle W, Krowczynski A (1983) *Chem Phys Lett* 101:291
- McMorrow D, Kasha M (1984) *J Phys Chem* 88:2235
- Martinez ML, Cooper WC, Chou P-T (1992) *Chem Phys Lett* 193:151
- Douhal A, Amat-Guerri V, Acuña AU (1995) *J Phys Chem* 99:76
- Chou PT, McMorrow D, Aartsma TJ, Kasha M (1984) *J Phys Chem* 88:4596
- Kim S, Park S-Y (2003) *Adv Mater* 15:1341
- Catalan J, del Valle JC, Claramunt RM, Sanz D, Dotor J and Lumin J (1996) 68: 165
- Parsapour F, Kelley DF (1996) *J Phys Chem* 100:2791
- Sytnik A, Kasha M (1994) *Proc Natl Acad Sci U S A* 91:8627
- Kim S, Seo J, Jung HK, Kim JJ, Park S-Y (2005) *Adv Mater* 17:2077
- Liu B, Wang H, Wang T, Bao Y, Du F, Tian J, Li Q, Bai R (2012) *Chem Commun* 48:2867
- Ding K, Courtney SJ, Strandjord AJ, Flom S, Friedrich D, Barbara PF (1983) *J Phys Chem* 87:1184–1188
- Harvey RG (1997) *Polycyclic aromatic compounds*. Wiley, New York
- Cook AH, Jones DH (1941) *J Chem Soc* 278–282
- Richard JP, Amyes TL (2001) *Curr Opin Chem Biol* 5:626–633
- Stoner-Ma D, Jaye AA, Ronayne KL, Nappa J, Meech SR, Tonge PJ (2008) *J Am Chem Soc* 130:1227–1235
- Jayabharathi J, Thanikachalam V, Jayamoorthy K (2013) Synthesis of some fluorescent benzimidazole derivatives using cobalt hydroxide (II) as high efficient catalyst—Spectral, physico-chemical studies and ESIPT process. *Photochem Photobiol Sci* 12:1761–1773
- Jayabharathi J, Thanikachalam V, Jayamoorthy K, Srinivasan N (2013) Synthesis, spectral studies and solvatochromism of some novel benzimidazole derivatives—ESIPT process. *Spectrochim Acta, Part A* 105:223–228
- Anbuselvan C, Jayabharathi J, Thanikachalam V, Tamilselvi G (2012) Physico-chemical studies on some fluorescence sensors: DFT based ESIPT process. *Spectrochim Acta, Part A* 97:125–130
- Jayabharathi J, Thanikachalam V, Jayamoorthy K (2012) Physicochemical studies of chemosensor imidazole derivatives: DFT based ESIPT process. *Spectrochim Acta, Part A* 89:168–176
- Jayabharathi J, Thanikachalam V, Vennila M, Jayamoorthy K (2012) Potential Fluorescent chemosensor based on L-Tryptophan derivative: DFT based ESIPT process. *Spectrochim Acta A* 95:446–451

42. Jayabharathi J, Thanikachalam V, Vennila M, Jayamoorthy K (2012) DFT based ESIPT process of luminescent chemosensor: taft and catalan solvatochromism. *Spectrochim Acta A* 95:589–595
43. Jayabharathi J, Thanikachalam V, Venkatesh Perumal M, Srinivasan N (2011) A physicochemical studies of azo dyes: DFT based ESIPT process. *Spectrochim Acta A* 83:200–206
44. Jayabharathi J, Thanikachalam V, Saravanan K, Venkatesh Perumal M (2011) Spectrofluorometric studies on the binding interaction of bioactive imidazole with bovine serum albumin: A DFT based ESIPT process. *Spectrochim Acta A* 79:1240–1246
45. Frisch MJ, Trucks GW, Schlegel HB, Scuseria GE, Robb MA, Cheeseman JR, Montgomery JA, Vreven T Jr, Kudin KN, Burant JC, Millam JM, Iyengar SS, Tomasi J, Barone V, Mennucci B, Cossi M, Scalmani G, Rega N, Petersson GA, Nakatsuji H, Hada M, Ehara M, Toyota K, Fukuda R, Hasegawa J, Ishida M, Nakajima T, Honda Y, Kitao O, Nakai H, Klene M, Li X, Knox JE, Hratchian P, Cross JB, Adamo C, Jaramillo J, Gomperts R, Stratmann RE, Yazyev O, Austin AJ, Cammi R, Pomelli C, Ochterski JW, Ayala PY, Morokuma K, Voth GA, Salvador P, Dannenberg JJ, Zakrzewski VG, Dapprich S, Daniels AD, Strain MC, Farkas O, Malick DK, Rabuck AD, Raghavachari K, Foresman JB, Ortiz JV, Cui Q, Baboul AG, Clifford S, Cioslowski J, Stefanov BB, Liu G, Liashenko A, Piskorz P, Komaromi I, Martin RL, Fox DJ, Keith T, Al-Laham MA, Peng CY, Nanayakkara A, Challacombe M, Gill PMW, Johnson B, Chen W, Wong MW, Gonzalez C, Pople JA (2004) Gaussian 03, Revision C.02. Gaussian, Wallingford
46. Tsai H-HG, Sun H-LS, Tan C-J (2010) TD-DFT study of the excited-state potential energy surfaces of 2-(2'-Hydroxyphenyl)-benzimidazole and its amino derivatives. *J Phys Chem A* 114:4065–4079
47. Wu Y, Peng X, Fan J, Gao S, Tian M, Zhao J, Sun S (2007) Fluorescence sensing of anions based on inhibition of excited-state intramolecular proton transfer. *J Org Chem* 72:62–70
48. Klymchenko AS, Demchenko AP (2002) *J Am Chem Soc* 124:12372–12379
49. Hsieh C-C, Jiang C-M, Chou P-T (2010) *Acc Chem Res* 43:1364–1374
50. Kakker R, Katoch V (2002) Theoretical study of the excited state intramolecular proton transfer in barbituric acid. *Theochem* 578:169–175
51. Park S, Kwon O-H, Kim S, Park S, Choi M-G, Cha M, Park SY, Jang D-J (2005) Imidazole-based excited-state intramolecular proton-transfer materials: synthesis and amplified spontaneous emission from a large single crystal. *J Am Chem Soc* 127:10070–10074
52. Park S, Kwon JE, Kim SH, Seo J, Chung K, Park S-Y, Jang D-J, Medina BM, Gierschner J, Park SY (2009) A white-light-emitting molecule: frustrated energy transfer between constituent emitting centers. *J Am Chem Soc* 131:14043–14049
53. Kim S, Chang DW, Park SY, Kawai H, Nagamura T (2002) Excited-state intramolecular proton transfer in a dendritic macromolecular system: Poly(aryl ether) dendrimers with phototautomerizable quinoline core. *Macromolecules* 35:2748–2753
54. Kim S, Zheng Q, He GS, Bharali DJ, Pudavar HE, Baev A, Prasad PN (2006) Aggregation-enhanced fluorescence and two-photon absorption in nanoaggregates of a 9,10-Bis[4'-(4"-aminostyryl)styryl]anthracene derivative. *Adv Funct Mater* 16:2317–2323
55. Silva GL, Ediz V, Yaron D, Armitage BA (2007) Experimental and computational investigation of unsymmetrical cyanine dyes: understanding torsionally responsive fluorogenic dyes. *J Am Chem Soc* 129:5710–5718
56. Kim S, Ohulchanskyy TY, Pudavar HE, Pandey RK, Prasad PN (2007) Organically modified silica nanoparticles co-encapsulating photosensitizing drug and aggregation-enhanced two-photon absorbing fluorescent dye aggregates for two-photon photodynamic therapy. *J Am Chem Soc* 129:2669–2675
57. Chen J, Xu B, Ouyang X, Tang BZ, Cao Y (2004) *J Phys Chem A* 108:7522–7526
58. Li Z, Dong Y, Mi B, Tang Y, Häussler M, Tong H, Dong Y, Lam JWY, Ren Y, Sung HH, Wong KS, Gao P, Williams ID, Kwok HS, Tang BZ (2005) *J Phys Chem B* 109:10061–10066
59. Tong H, Hong Y, Dong Y, Ren Y, Häussler M, Lam JWY, Wong KS, Tang V (2007) *J Phys Chem B* 111:2000–2007
60. Vázquez SR, Rodríguez MCR, Mosquera M, Rodríguez-Prieto F (2007) *J Phys Chem A* 111:1814–1826
61. Paul BK, Mahanta S, Singh RB, Guchhait N (2010) A DFT based theoretical study on the photophysics of 4-hydroxyacridine: Single-water-mediated excited state proton transfer. *J Phys Chem A* 114:2618–2627
62. Wu K-C, Ku P-J, Lin C-S, Shih H-T, Wu F-I, Huang, Lin J-J, Chen I-C, Cheng C-H (2008) The photophysical properties of dipyrrenylbenzenes and their application as exceedingly efficient blue emitters for electroluminescent devices. *Adv Funct Mater* 18:67–75
63. Dey J, Roberts EL, Warner IM (1998) *J Phys Chem A* 102:301–305
64. Saha SK, Dogra SK (1998) *J Mol Struct* 470:301–311
65. Purkayastha P, Bera SC, Chattopadhyay N (2000) *J Mol Liq* 88:33–42
66. Saha SK, Pandey S, Dogra SK (1995) *Indian J Chem* 34A:771–777
67. Swaminathan M, Dogra SK (1983) *J Am Chem Soc* 105:6223–6228
68. Fayed TA, Ali SS (2003) *Spectrosc Lett* 36:375–386
69. Stewart JJP (1989) *J Comput Chem* 10: 221–264, 209–220
70. Bottcher CJF (1983) Theory of electronic polarization, vol 1. Elsevier, Amsterdam
71. Gorse A-D, Pesquer M (1995) *J Phys Chem* 99:4039–4049
72. Purkayastha P, Chattopadhyay N (2000) *Phys Chem Chem Phys* 2: 203–210
73. Purkayastha P, Chattopadhyay N (2003) *Int J Mol Sci* 4:335–361
74. Grabowski ZR, Rotkiewicz K, Siemiarczuk A, Cowley DJ, Baumann W (1979) *Nouv J Chim* 3:443–454
75. Kato S, Amatatsu Y (1990) *J Chem Phys* 92:7241–7257
76. Lipinski J, Chojnacki H, Grabowski ZR, Rotkiewicz K (1980) *Chem Phys Lett* 70:449–453
77. Marguet S, Mialocq JC, Millie P, Berthier G, Momicchioli F (1992) *Chem Phys* 160:265–279
78. LaFemina JP, Duke CB, Paton A (1987) *J Chem Phys* 87:2151–2157
79. Steiger D, Ahlbrandt C, Glaser R (1998) *J Phys Chem B* 102:4257–4260
80. Nikolaev AE, Myszkiewicz G, Berden G, Meerts WL, Pfanstiel JF, Pratt DW (2005) *J Chem Phys* 122: 084309-1-10
81. Grabowski ZR, Rotkiewicz K, Retting W (2003) *Chem Rev* 103: 3899–4032
82. Amamatsu Y (2000) *Theor Chem Acc* 103:445–450